Exp. Anim. 67(2), 201–218, 2018

—Original—

Deletion of both *p62* and *Nrf2* spontaneously results in the development of nonalcoholic steatohepatitis

Kentaro AKIYAMA[1,2)]*, Eiji WARABI[3)]*, Kosuke OKADA[4)], Toru YANAGAWA[5)], Tetsuro ISHII[3)], Katsumi KOSE[6)], Katsutoshi TOKUSHIGE[7)], Kazunori ISHIGE[4)], Yuji MIZOKAMI[4)], Kenji YAMAGATA[5)], Kojiro ONIZAWA[5)], Shun-ichi ARIIZUMI[8)], Masakazu YAMAMOTO[8)], and Junichi SHODA[9)]

[1)]*Doctoral Programs in Medical Sciences, Graduate School of Comprehensive Human Sciences, University of Tsukuba, 1-1-1 Tennodai, Tsukuba-shi, Ibaraki 305-8575, Japan*
[2)]*Japan Society for the Promotion of Science, 5-3-1 Kojimachi, Chiyoda-ku, Tokyo 102-0083, Japan*
[3)]*Division of Biomedical Science, Faculty of Medicine, University of Tsukuba, 1-1-1 Tennodai, Tsukuba-shi, Ibaraki 305-8575, Japan*
[4)]*Division of Gastroenterology, Faculty of Medicine, University of Tsukuba, 1-1-1 Tennodai, Tsukuba-shi, Ibaraki 305-8575, Japan*
[5)]*Division of Oral and Maxillofacial Surgery, Faculty of Medicine, University of Tsukuba, 1-1-1 Tennodai, Tsukuba-shi, Ibaraki 305-8575, Japan*
[6)]*Institute of Applied Physics, University of Tsukuba, 1-1-1 Tennodai, Tsukuba-shi, Ibaraki 305-8573, Japan*
[7)]*Institute of Gastroenterology Internal Medicine, Tokyo Women's Medical University, 8-1 Kawada-cho, Shinjuku-ku, Tokyo 162-8666, Japan*
[8)]*Institute of Gastroenterology Surgery, Tokyo Women's Medical University, 8-1 Kawada-cho, Shinjuku-ku, Tokyo, 162-8666, Japan*
[9)]*Medical Sciences, Faculty of Medicine, University of Tsukuba, 1-1-1 Tennodai, Tsukuba-shi, Ibaraki 305-8575, Japan*

Abstract: Nonalcoholic steatohepatitis (NASH) is one of the leading causes of chronic liver disease worldwide. However, details of pathogenetic mechanisms remain unknown. Deletion of both *p62/Sqstm1* and *Nrf2* genes spontaneously led to the development of NASH in mice fed a normal chow and was associated with liver tumorigenesis. The pathogenetic mechanism (s) underlying the NASH development was investigated in *p62:Nrf2* double-knockout (DKO) mice. DKO mice showed massive hepatomegaly and steatohepatitis with fat accumulation and had hyperphagia-induced obesity coupled with insulin resistance and adipokine imbalance. They also showed dysbiosis associated with an increased proportion of gram-negative bacteria species and an increased lipopolysaccharide (LPS) level in feces. Intestinal permeability was elevated in association with both epithelial damage and decreased expression levels of tight junction protein zona occludens-1, and thereby LPS levels were increased in serum. For Kupffer cells, the foreign body phagocytic capacity was decreased in magnetic resonance imaging, and the proportion of M1 cells was increased in DKO mice. *In vitro* experiments showed that the inflammatory response was accelerated in the *p62*:*Nrf2* double-deficient Kupffer cells when challenged with a low dose of LPS. Diet restriction improved the hepatic conditions of NASH in association with improved dysbiosis and decreased LPS levels. The results suggest that in DKO mice, activation of innate immunity by excessive LPS flux from the intestines, occurring both within and outside the liver, is central to the development of hepatic damage in the form of NASH.
Key words: dysbiosis, hyperphagia, intestinal permeability, lipopolysaccharide, multiple parallel hits hypothesis

(Received 20 September 2017 / Accepted 28 November 2017 / Published online in J-STAGE 25 December 2017)

**These authors contributed equally to this work.*

Address corresponding: J. Shoda, Medical Sciences, Faculty of Medicine, University of Tsukuba, 1-1-1 Tennoudai, Tsukuba-shi, Ibaraki 305-8575, Japan

Supplementary Figures and Tables: refer to J-STAGE: https://www.jstage.jst.go.jp/browse/expanim

Introduction

Nonalcoholic steatohepatitis (NASH) is a progressive liver disease characterized by steatosis, inflammation, and fibrosis leading to liver cirrhosis and cancer [3]. NASH, a hepatic representation of metabolic syndrome, is an increasingly common health problem globally [40].

It is unlikely that the pathogenesis of NASH is dependent upon any single factor, and it is likely that NASH is the result of multiple factors, including obesity/insulin resistance-mediated steatosis, intestinal-derived lipopolysaccharides (LPS), oxidative stress, lipotoxicity, and other conditions that promote inflammation, fibrosis, and hepatocyte death [7, 38]. The molecular mechanisms corresponding to these pathogenic processes are poorly understood.

p62/A170/Sqstm1 is a cytoplasmic endosome-associated protein that acts as a scaffold for atypical protein kinase C [17]. Recently, p62 was reported to play an important role in selective autophagy of ubiquitin-binding protein [24, 35]. *p62*-knockout (*p62*-KO) mice develop mature-onset obesity after progressing to insulin and leptin resistance when fed a standard diet [33]. In a previous study, hyperphagia (overeating) was reported to be the primary cause of obesity in *p62*-KO mice and was found to be associated with a disruption in leptin signaling [12].

Nuclear factor E2-related factor-2 (Nrf2), a transcription factor, is a master regulator of the cellular adaptive response to oxidative stress [19, 23, 37]. *Nrf2*-knockout (*Nrf2*-KO) mice exhibit a severe deficiency in the gene regulatory program for the antioxidant response, resulting in high susceptibility to oxidative stress-related disorders and chemical carcinogenesis [20]. In a previous study, *Nrf2*-KO mice were found to be prone to developing NASH/fatty liver disease when fed a diet deficient in methionine and choline [32]. It is reported that activation of Nrf2 prevents LPS-induced transcriptional upregulation of pro-inflammatory cytokines, including interleukin (Il)-6 and IL-1β [22].

Recent animal models of NASH include a diet-induced rat model developed by administration of a methionine- and choline-deficient diet and hepatocyte-specific Pten-deficient mice [15, 45]. However, these animal models show an unnatural decrease in body weight and rapid progression of symptoms, and there is the possibility that they deviate from human NASH. The lack of comparative animal models is a major reason for why the pathogenic mechanisms of NASH have not been clarified, and the development of a novel model is required.

In the current study, we developed a *p62*:*Nrf2* gene double-knockout (DKO) mouse by crossing a *p62*-KO mouse and an *Nrf2*-KO mouse and investigated possible new mechanisms associated with the deletion of both *p62* and *Nrf2* genes in the pathogenesis of NASH. It is likely that p62 and Nrf2 deficiency plays a variety of pathogenic roles in a number of organs and/or tissues that form a basis for NASH onset and progression through a linkage between organs and tissues. We found that the DKO mouse is a novel animal model of NASH.

Materials and Methods

Animal studies

All experiments were performed under protocols approved by the Institutional Animal Care and Use Committees of the University of Tsukuba. Except where indicated in this paper or cited in the respective references, animals were bred and maintained under standard housing conditions with *ad libitum* access to food (MF: 5.1% fat, 23.1% protein, 360 kcal/100 g; Oriental Yeast, Tokyo, Japan) and water. They were housed at an ambient temperature of 20–23°C on a daily 12-h light/dark cycle with 30–70% relative humidity and were weaned from their mothers between 3–4 weeks of age. All mice were kept under specific pathogen-free conditions in an environmentally controlled clean room at the Laboratory Animal Resource Center, University of Tsukuba.

The mice used were 8-, 30-, and 50-week-old male wild-type (WT) C57BL/6J mice obtained from Charles Laboratories Japan (Kanagawa, Japan) and bred in our own colony. *p62*-KO and *Nrf2*-KO mice were generated and genotyped as previously described [18, 24]. DKO mice were produced by crossing these mutant mice and regenotyped. Before analysis, mice were crossed with C57BL/6J mice for>10 generations to produce fertile offspring that grew normally. Male mice were used in all experiments. In pair-feeding experiments, one 3-week-old DKO pup was weaned in a separate cage and given a portion of standard diet (3.0 ± 0.1 g) per day until 25 weeks of age [12]. In probiotics experiments, DKO mice were administered probiotics (VSL#3, VSL Pharmaceuticals, Gaithersburg, MD, USA) from 10 weeks of age and observed at 25 weeks of age. VSL#3 was dissolved in drinking water (4.5 billion colonies/ml).

Glucose tolerance test

Mice were fasted for 13 h before intraperitoneal injection of glucose (1 g/kg body weight). A drop of blood drop was taken from the tail after 15, 30, 60, and 120 min. The tail tip was cut 2 mm from the end, and the tail was pressed to collect a drop of blood at the indicated time. Glucose levels were measured using a portable glucose meter (Ascensia, Bayer HealthCare, Berlin, Germany).

Biochemical analyses

Serum glucose was detected using a glucose CII test kit (Wako, Tokyo, Japan). Serum insulin was measured using a mouse insulin ELISA kit (Morinaga, Kanagawa, Japan). Serum leptin was measured using a mouse/rat leptin ELISA kit (Morinaga, Kanagawa, Japan). Adiponectin was measured in serum using a Mouse Adiponectin/Acrp30 Quantikine ELISA Kit (R&D Systems, Minneapolis, MN, USA). The homeostatic model assessment for insulin resistance (HOMA-IR) was determined by performing the following calculation: HOMA-IR=fasting plasma insulin (mU/l) × fasting blood glucose (mg/dl)/405.

Histological analysis

Liver, intestine, and adipose tissues were fixed in 4% paraformaldehyde and embedded in paraffin, and 2 μm-thick tissue sections were stained with hematoxylin-eosin (H&E) and sirius red solution. For immunostaining of 4-hydroxy-2-nonenal (4-HNE), sections were stained using the indirect immunoperoxidase method with anti-4HNE monoclonal antibodies (Ab) (JaiCA, Shizuoka, Japan). For immunostaining of glutathione S-transferase P1, tissue sections were immunostained with mAb (BML, Tokyo, Japan). To determine the histopathological lesions in nonalcoholic fatty liver disease, the steatosis, activity, and fibrosis (SAF) score were assessed separately for the grade of steatosis (from S0 to S3), the activity (from A0 to A4 by adding grades of ballooning and lobular inflammation, both from 0 to 2), and the stage of fibrosis (from F0 to F4) [2]. Histological changes in the intestines were evaluated and graded by a blinded evaluator as follows: 0 (normal), no damage; 1 (mild), slight submucosal and/or lamina propria separation; 2 (moderate), moderate separation of the submucosa and/or lamina propria and/or edema in the submucosa and muscular layers; 3 (severe), severe separation of the submucosa and/or lamina propria and/or severe edema in the submucosa and muscular layers with regional villous sloughing; and 4 (necrosis), loss of villi and necrosis [28].

LPS levels

Concentrations of LPS in plasma and feces were evaluated using a Pyrochrome limulus amebocyte lysate assay (Associates of Cape Cod, East Falmouth, MA, USA). LPS levels are expressed as Endotoxin Units (EU).

Fecal bacterial analysis

Stool samples were collected from mice, snap-frozen and stored at −80°C until use. DNA extraction from fecal samples and analysis of the fecal microbiota using a 16S rDNA library and terminal restriction fragment length polymorphisms were outsourced to TechnoSuruga Laboratory Co., Ltd. (Shizuoka, Japan). Preparation of the fecal microbiota using a 16S rRNA gene amplicon library and analysis of 16S rRNA gene amplicon sequencing were outsourced to FASMAC Co., Ltd. (Kanagawa, Japan).

Magnetic resonance imaging (MRI) analyses

For analysis of Kupffer cells phagocytosis, MRI was performed using a 1T animal scanner (MRTechnology, Ibaraki, Japan). Region-of-interest measurements of T2 values were performed on consecutive pre- and superparamagnetic iron oxide (SPIO) administration.

Evaluation of microsphere phagocytosis

Prior to 5 min of liver perfusion, latex beads (1.0 μm diameter, carboxylate-modified; FluoSpheres®, Thermo Fisher Scientific, Waltham, MA, USA) at 0.57 μl/g body weight were injected into the tail vein. Following liver perfusion, cells were isolated. The Kupffer cell surface marker F4/80 was stained. The percentage of phagocytic cells and the fluorescence intensity of latex beads in F4/80-positive cells were evaluated by flow cytometry.

Flow cytometric analysis

Kupffer cells were stained with APC-conjugated anti-F4/80 Ab (Thermo Fisher Scientific, Waltham, MA, USA), PerCP/Cy5.5 anti-mouse CD206 Ab (BioLegend, San Diego, CA, USA), PE anti-mouse CD11c Ab (Biolegend, CA, USA), anti-macrophage receptor with collagenous structure (MARCO) Ab (Bio-Rad, Hercules, CA, USA), and anti-class A macrophage scavenger re-

ceptor (SR-A) Ab (R&D Systems, Minneapolis, MN, USA) with Alexa Fluor 488 (Thermo Fisher Scientific, Waltham, MA, USA). Flow cytometry was performed using a Gallios flow cytometer (Beckman Coulter, Brea, CA, USA).

Intestinal permeability assay

To evaluate epithelial permeability in the intestines, mice underwent gavage with nondigestible 4 kDa fluorescein isothiocyanate (FITC)-dextran (Sigma-Aldrich, St. Louis, MO, USA) at a dose of 0.5 mg/g body weight after fasting for 13 h. Serum (50 μl) was collected from the fundus at various time points (0, 1, 2, 3, and 6 h), and the intensity of FITC in serum was measured using an iMark plate reader (Bio-Rad, Hercules, CA, USA) with excitation at 488 nm. Data were plotted against the standard curve of serial dilutions of FITC-dextran.

Immunoblot analysis

After extraction from mouse samples or cultured cells, each protein sample was subjected to SDS/PAGE and transferred to a PVDF membrane (Bio-Rad, Hercules, CA, USA). Then the corresponding primary and secondary antibodies were incubated to visualize the protein. All antibodies used in this study are listed in Supplementary Table 1.

Quantitative real-time polymerase chain reaction (qRT-PCR)

Total RNA was extracted from specimens or cultured cells, followed by cDNA synthesis. qRT-PCR was performed with Fast SYBR Green Master Mix (Thermo Fisher Scientific, Waltham, MA, USA). Data were normalized to the amount of Glyceraldehyde 3-phosphate dehydrogenase (*GAPDH*) present in each sample and then averaged. Supplementary Table 2 provides a list of all the primers used in this study.

In vitro tissue culture studies and cell lines

Mouse primary Kupffer cells from 8- to 10-week-old male WT, *Nrf2*-KO, *p62*-KO, and DKO mice were isolated via portal vein collagenase treatment (Worthington Biochemical, Lakewood, NJ, USA) followed by centrifugation and cell sorting. For Kupffer cell sorting, cells were incubated with APC-conjugated anti-F4/80 Abs (Thermo Fisher Scientific, Waltham, MA, USA) for 30 min. Cells were sorted into $F4/80^+$ subpopulations using a Beckman Coulter MoFlo XDP cell sorter and immediately processed for RNA isolation.

The murine monocyte/macrophage cell line RAW264.7 was obtained from ATCC. The human colon cancer cell line Caco-2 was purchased from RIKEN BRC (Ibaraki, Japan). Cells were cultured at 37°C under 5% CO_2 in high glucose Dulbecco's modified Eagle's medium containing 4.5 g/l glucose, 1% penicillin-streptomycin, 10% fetal bovine serum, and 1% nonessential amino acids (only in Caco-2).

Knockout of p62 and Nrf2 genes using the CRISPR-Cas9 system

The detailed instructions of a published protocol were followed to knock out p62 and Nrf2 genes using the CRISPR-Cas9 system [5]. Briefly, 20 bp target single-guide RNA sequences were obtained by screening *p62* and *Nrf2* mRNA sequences using the CRISPR Design online software (http://crispr.mit.edu/). After annealing, short double-strand DNA was ligated using the *Bbs*I digested pX330 plasmid. RAW264.7 and Caco-2 cells were transfected with individual pX330 gDNA using the Neon Transfection System.

Measurement of transepithelial electrical resistance (TER)

Caco-2 cells were seeded into a polyethylene terephthalate membrane with 0.4 μm pores. The medium was changed every other day until complete differentiation. Electrical resistance was measured using a Millicell-ERS electrical resistance system (EMD Millipore, Billerica, MA, USA). TER values are expressed as $\Omega \cdot cm^2$. Measurements were performed on three replicates in three independent experiments. In the LPS experiments, cell monolayers were treated with 100 EU / ml LPS for 3 or 6 h, and TER was measured.

Statistical analysis

Statistical analysis was conducted using IBM SPSS Statistics 22.0 (IBM, Armonk,, NY, USA). Values are expressed as the mean ± SE. When two groups were compared, the unpaired *t*-test was used for data analysis. Multiple-group comparisons were performed using one-way analysis of variance (ANOVA). A P-value<0.05 was considered statistically significant.

Results

DKO mice fed a normal chow diet exhibited hyperphagia, obesity, insulin resistance, and adipokine imbalance

DKO mice were negative for p62 and Nrf2 protein expression in the liver (Fig. 1A). The body weights of WT, *Nrf2*-KO, *p62*-KO, and DKO mice fed a normal chow diet were monitored over a 42-week period in mice 8–50 weeks of age. Mice lacking *p62* and/or *Nrf2* genes were viable and had similar body weights at birth. Thereafter, *p62*-KO and DKO mice gained weight much faster than WT and *Nrf2*-KO mice (Fig. 1B). At 30 weeks of age, the body weights for each genotype were 37.8 ± 1.3 g for WT, 37.6 ± 1.0 g for *Nrf2*-KO, 49.7 ± 1.3 g for *p62*-KO, and 46.5 ± 0.6 g for DKO. Liver mass was significantly increased in DKO mice compared with in WT mice (Supplementary Fig. 1A) but was less than that in *p62*-KO mice. Using computed tomography, percentages of body fat and visceral fat weight were observed to increase in *p62*-KO and DKO mice (Supplementary Fig. 1B). WT and *Nrf2*-KO mice showed only a slight increase in food intake with age, with the average intake at 8 weeks being 3.0 g/day/mouse. In contrast, food intake of *p62*-KO and DKO mice increased from 3.3 g/day/mouse at 8 weeks of age to 4.0 g/day/mouse at 30 weeks of age (Fig. 1C).

In comparisons of blood biochemistry versus the WT mice, DKO mice showed the development of hyperglycemia and a tendency towards increased fasting insulin levels and homeostatic model assessment for insulin resistance (HOMA-IR). Of note, DKO mice exhibited insulin resistance at 8 weeks of age (Fig. 1D). In addition, DKO mice exhibited glucose intolerance in an intraperitoneal glucose tolerance test (Fig. 1E). Serum leptin levels in *p62*-KO and DKO mice increased significantly from 8 weeks to 30 weeks of age compared with WT and *Nrf2*-KO mice. Serum adiponectin levels in *p62*-KO and DKO mice decreased significantly (Fig. 1F).

Collectively, the results indicated that DKO mice developed hyperphagia and obesity (visceral fat accumulation) and exhibited insulin resistance and adipokine imbalance.

DKO mice fed a normal chow diet developed NASH and liver tumors

The time course of changes in liver histology for WT, *Nrf2*-KO, *p62*-KO, and DKO mice are shown in Figs. 2A, 2B, and Supplementary Fig. 2A *p62*-KO and DKO mice exhibited steatosis at 30 weeks of age (Fig. 2C). DKO mice showed a marked increase in infiltration of inflammatory cells in the liver compared with WT mice (Fig. 2D). Hepatic fibrosis significantly increased in DKO mice (Fig. 2E). In contrast, no marked increase in hepatic fibrosis was observed in *Nrf2*-KO and *p62*-KO mice (Fig. 2E). The extent of fibrosis was confirmed by Masson's trichrome staining and was closely associated with hepatic fibrosis (Fig. 2F). While steatosis, activity, and fibrosis (SAF) scores increased in *Nrf2*-KO and *p62*-KO mice, scores showed greater increases in DKO mice (Fig. 2C-E). Immunostaining with 4-HNE was performed to determine the presence of lipid peroxides. Increased staining was observed in the livers of DKO mice at 30 weeks of age but not in *Nrf2*-KO and *p62*-KO mice (Supplementary Fig. 2B).

Tumor formation was observed in the livers of DKO mice. Macroscopic liver tumors were observed in 12% (8/66) of DKO mice by 50 weeks of age (Fig. 2G). No tumors were observed in *Nrf2*-KO and *p62*-KO mice. Microscopic findings revealed that tumors were comprised of cellular masses with nuclear atypia, included lipid droplets in some cells, and were partially surrounded by a fibrous cap. Intense glutathione S-transferase P1 staining was observed in whole sections of tumors.

With regard to visceral fat tissue, crown-like structures of inflammatory cells, comprising macrophages surrounding dead or dying adipocytes (a histologic hallmark of the pro-inflammatory process), were observed in *p62*-KO and DKO mice, with greater inflammatory cell infiltration being observed in DKO mice (Supplementary Fig. 2C).

Hepatic expression levels of tumor necrosis factor-α (*Tnf-α*), *IL-1β*, *IL-6*, and toll-like receptor 4 (*Tlr4*) mRNA increased in DKO mice at 8 and 30 weeks of age compared with WT mice. mRNA levels of transforming growth factor-β1 (*Tgf-β1*) and procollagen-α1, both of which are closely associated with hepatic fibrosis, increased in DKO mice at 30 weeks of age (Table 1). Visceral fat expression levels of *IL-1β* mRNA significantly increased in DKO mice at 8 weeks of age. mRNA levels of *Tnf-α*, *IL-1β*, *Tlr4*, monocyte chemoattractant protein 1 (*Mcp-1*), *CD14*, and *Tgf-β1* increased in DKO mice at 30 weeks of age compared with WT mice (Table 1).

These results suggested that DKO mice first developed liver inflammation at an early age prior to obesity and then developed NASH and liver tumors with aging.

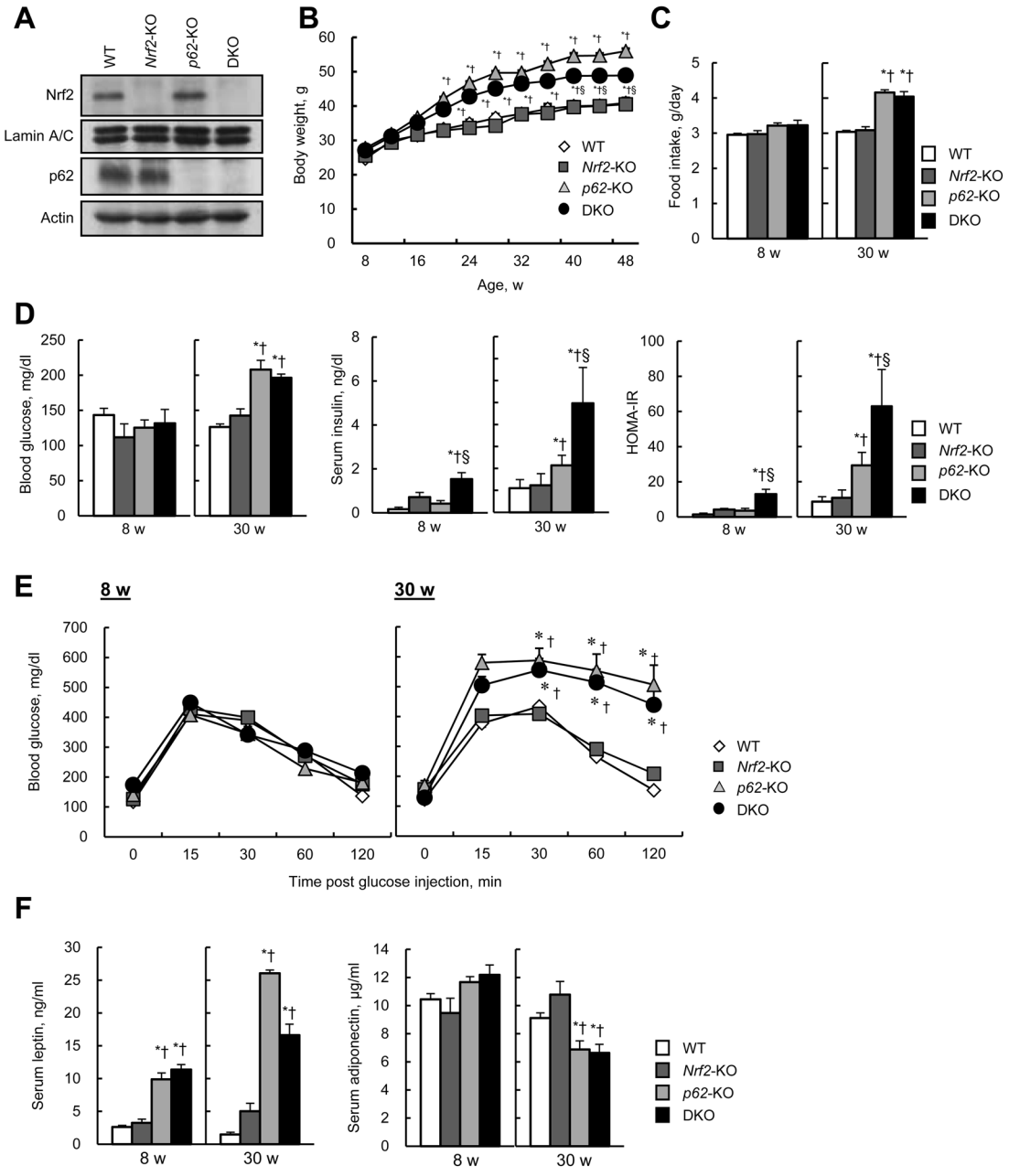

Fig. 1. *p62*:*Nrf2* gene double-knockout (DKO) mice fed a normal chow diet exhibited hyperphagia, obesity, insulin resistance, and adipokine imbalance. (A) Immunoblot analysis of Nrf2 and p62 in livers of wild-type (WT), *Nrf2*-knockout (KO), *p62*-KO, and DKO mice at 8 weeks of age. (B) Body weight changes in WT, *Nrf2*-KO, *p62*-KO, and DKO mice (n=10–15 per group). (C) Food intake, (D) fasting blood glucose concentration, fasting serum insulin concentration, and homeostatic model assessment for insulin resistance (HOMA-IR) (n=8 per group) at 8 and 30 weeks of age. (E) Glucose tolerance tests were performed after mice were fasted for 13 h at 8 and 30 weeks of age (n=7–9 per group). (F) Serum leptin and adiponectin concentrations at 8 and 30 weeks of age (n=8 per group). Results are presented as the mean ± SE. **P*<0.05, significantly different from the WT group; †*P*<0.05, significantly different from the *Nrf2*-KO group; §*P*<0.05, significantly different from the *p62*-KO group.

Modified microbiota composition and fecal LPS content in DKO mice

Fecal microbiota composition was determined in DKO mice at 30 weeks of age. Analysis was conducted using culture-independent PCR amplification of the variable 4 region of bacterial 16S rRNA genes followed by Illumina sequencing. Principal coordinates analysis of the weighted UniFrac distance between samples revealed

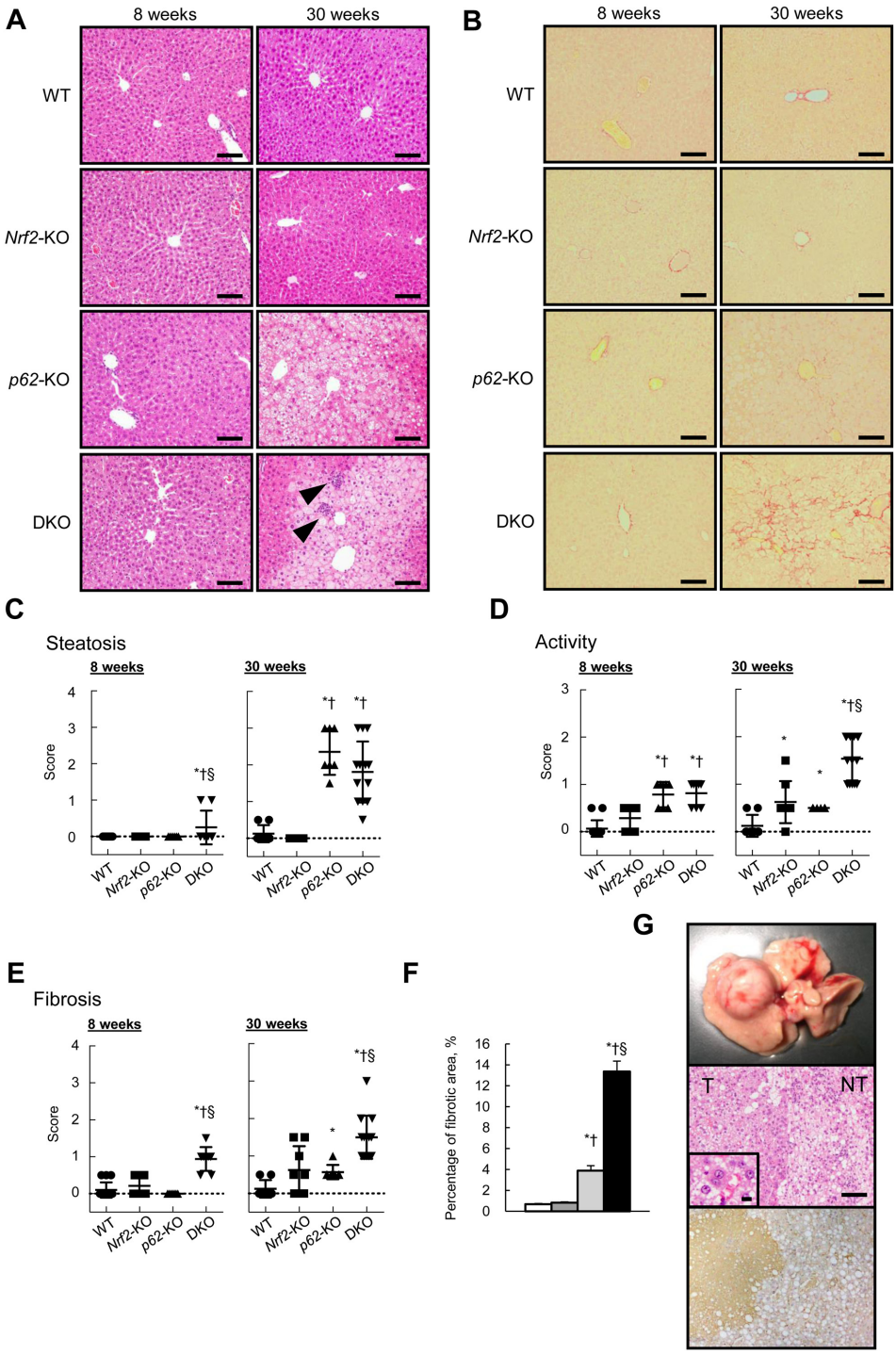

Fig. 2. *p62*:*Nrf2* gene double-knockout (DKO) mice developed nonalcoholic steatohepatitis and liver tumors. (A) Hematoxylin and eosin (H&E)-stained sections of representative liver specimens from wild-type (WT), *Nrf2*-knockout (KO), *p62*-KO, and DKO mice at 8 and 30 weeks of age. Arrowheads indicate infiltration of inflammatory cells (scale bar, 100 μm). (B) Sirius red-stained sections. (C–E) The steatosis, activity, and fibrosis (SAF) scores for each group are shown (n=8 per group). (F) Fibrotic areas in livers of WT, *Nrf2*-KO, *p62*-KO, and DKO mice (n=8 per group). (G) Representative liver tumors in DKO mice. Macroscopic view of tumors (upper panel), an H&E-stained section (middle panel; T, tumor part; NT, non-tumor part), and a glutathione S-transferase P1-stained section of the tumor (lower panel) (scale bar, 100 μm). The inset areas show magnified views of part of the tumor in the middle panels (scale bar, 10 μm). Results are presented as the mean ± SE. **P*<0.05, significantly different from the WT group; †*P*<0.05, significantly different from the *Nrf2*-KO group; §*P*<0.05, significantly different from the *p62*-KO group.

Table 1. Relative mRNA expression levels determined by qPCR for pathophysiological factors in the liver and visceral fat tissue of mice at 8 and 30 weeks of age

Age	8 weeks				30 weeks			
Genes	WT	*Nrf2*-KO	*p62*-KO	DKO	WT	*Nrf2*-KO	*p62*-KO	DKO
Liver								
Tnf-α	1.00 ± 0.10	1.11 ± 0.17	1.60 ± 0.07 [a]	3.09 ± 0.84 [ab]	2.47 ± 0.79	3.02 ± 0.70	4.25 ± 0.37 [ab]	5.43 ± 1.01 [ab]
IL-1β	1.00 ± 0.17	0.85 ± 0.08	2.69 ± 0.31 [ab]	3.52 ± 0.41 [ab]	1.68 ± 0.26	2.02 ± 0.15	3.19 ± 0.36 [ab]	4.18 ± 0.32 [ab]
IL-6	1.00 ± 0.25	1.27 ± 0.07	2.99 ± 0.32 [ab]	2.49 ± 0.28 [ab]	1.39 ± 0.57	0.97 ± 0.32	2.66 ± 0.77 [ab]	4.14 ± 0.96 [ab]
Tlr-4	1.00 ± 0.17	1.16 ± 0.06	1.09 ± 0.09	1.43 ± 0.12 [abc]	1.69 ± 0.23	1.82 ± 0.29	4.02 ± 0.35 [ab]	3.84 ± 0.43 [ab]
Tgf-β1	1.00 ± 0.15	1.07 ± 0.08	0.86 ± 0.05	1.35 ± 0.15	0.97 ± 0.71	0.98 ± 0.36	1.49 ± 0.61	1.82 ± 0.72 [ab]
Procollagen-α1	1.00 ± 0.16	1.26 ± 0.23	0.83 ± 0.13	1.24 ± 0.19	1.14 ± 0.73	1.30 ± 0.65	1.88 ± 0.39	2.27 ± 0.79 [a]
Visceral fat								
Tnf-α	1.00 ± 0.10	1.17 ± 0.27	0.80 ± 0.10	1.30 ± 0.30	1.15 ± 0.26	1.23 ± 0.45	2.48 ± 0.22	5.72 ± 0.78 [abc]
IL-1β	1.00 ± 0.16	1.47 ± 0.61	1.60 ± 0.34	4.10 ± 0.86 [abc]	1.92 ± 0.52	6.92 ± 2.14	4.20 ± 1.22	32.26 ± 12.83 [abc]
Tlr-4	1.00 ± 0.06	0.93 ± 0.16	0.88 ± 0.11	0.81 ± 0.02	0.90 ± 0.08	0.98 ± 0.15	0.89 ± 0.08	1.66 ± 0.18 [abc]
Mcp-1	1.00 ± 0.11	2.26 ± 0.54	1.40 ± 0.20	1.75 ± 0.46	1.09 ± 0.12	1.31 ± 0.38	3.70 ± 1.11	15.55 ± 4.84 [abc]
Cd14	1.00 ± 0.18	0.64 ± 0.17	0.65 ± 0.13	0.48 ± 0.06	0.63 ± 0.04	0.70 ± 0.10	0.99 ± 0.27	3.29 ± 0.99 [abc]
Tgf-β1	1.00 ± 0.12	0.91 ± 0.13	0.85 ± 0.06	0.79 ± 0.07	0.65 ± 0.04	0.81 ± 0.14	0.82 ± 0.12	1.68 ± 0.15 [abc]

mRNA expression levels were normalized using the values of the WT group at 8 weeks of age. Values are presented as the mean ± SE (n=8 per group). [a]$P<0.05$, significantly different from the WT group; [b]$P<0.05$, significantly different from the *Nrf2*-KO group; [c]$P<0.05$, significantly different from the *p62*-KO group. DKO, *p62:Nrf2* gene double-deficient mice; Tnf, tumor necrosis factor; Tlr, toll-like receptor; Mcp, monocyte chemotactic protein; Cd, cluster of differentiation; Tgf, transforming growth factor.

that the microbiota composition was profoundly modified in DKO mice (Fig. 3A). Whereas gram-positive bacteria were the major representative signature operational taxonomic unit accounting for the differences in intestinal microbiota composition in WT mice, gram-negative bacteria were the predominant signature operational taxonomic unit in *p62*-KO and DKO mice (Fig. 3B). The *Porphyromonadaceae* and *Paraprevotellaceae* families were more abundant in DKO than in WT mice, and the *Lachnospiraceae* and *Ruminococcaceae* families were less abundant in DKO mice (Fig. 3C).

LPS is the predominant cause of liver inflammation in NASH patients [4, 46]. Therefore, fecal and serum levels of LPS were determined in mice. Correlating with the microbiota composition, fecal LPS concentrations were higher in *p62*-KO and DKO mice than in WT mice (Fig. 3D), but serum LPS concentrations were higher only in DKO mice (Fig. 3E).

Intestinal permeability increased in DKO mice

Previous studies have reported that increased intestinal permeability is observed more frequently in NASH patients [30, 34]. In the current study, intestinal tissue sections from WT, *Nrf2*-KO, *p62*-KO, and DKO mice were stained with hematoxylin and eosin, and epithelial damage was scored according to the histology. There was marked damage to intestinal epithelial morphology in DKO mice compared with WT mice. At 30 weeks, damage scores increased in *Nrf2*-KO and *p62*-KO mice, but they increased to a greater extent in DKO mice (Fig. 4A). Measurement of intestinal permeability by absorption of FITC-dextran showed prominent enhancement in *Nrf2*-KO and DKO mice compared with WT at 8 weeks of age. Permeability in DKO mice was further increased at 30 weeks of age (Fig. 4B).

Intestinal permeability is regulated by tight junctions formed between intestinal epithelial cells at most apical areas of the epithelium. Expression levels of the tight junction protein zona occludens-1 (Zo-1) were evaluated by immunoblotting of intestinal tissue lysates from DKO mice. Expression levels of Zo-1 decreased in the intestines of *Nrf2*-KO and DKO mice compared with WT mice (Fig. 4C). Expression levels of Claudin 1 and Claudin 2 were not significantly different among the groups of mice (data not shown). mRNA expression levels of intestinal *Zo-1*, *Claudin 1*, and *Claudin 2* were also not significantly different (Supplementary Fig. 3A).

To investigate the effects of *p62* or *Nrf2* deficiency on intestinal barrier function, an *in vitro* model in which Caco-2 epithelial cells were grown in monolayers was constructed. Using the CRISPR-Cas9 system, Caco-2 cells lacking the *p62* or *Nrf2* gene were also constructed. Expression of p62 and Nrf2 protein in each gene-deficient cell was confirmed by immunoblotting (Fig. 4D). TER is an indicator of epithelial paracellular permeability to ionic solutes and was used to assess intestinal bar-

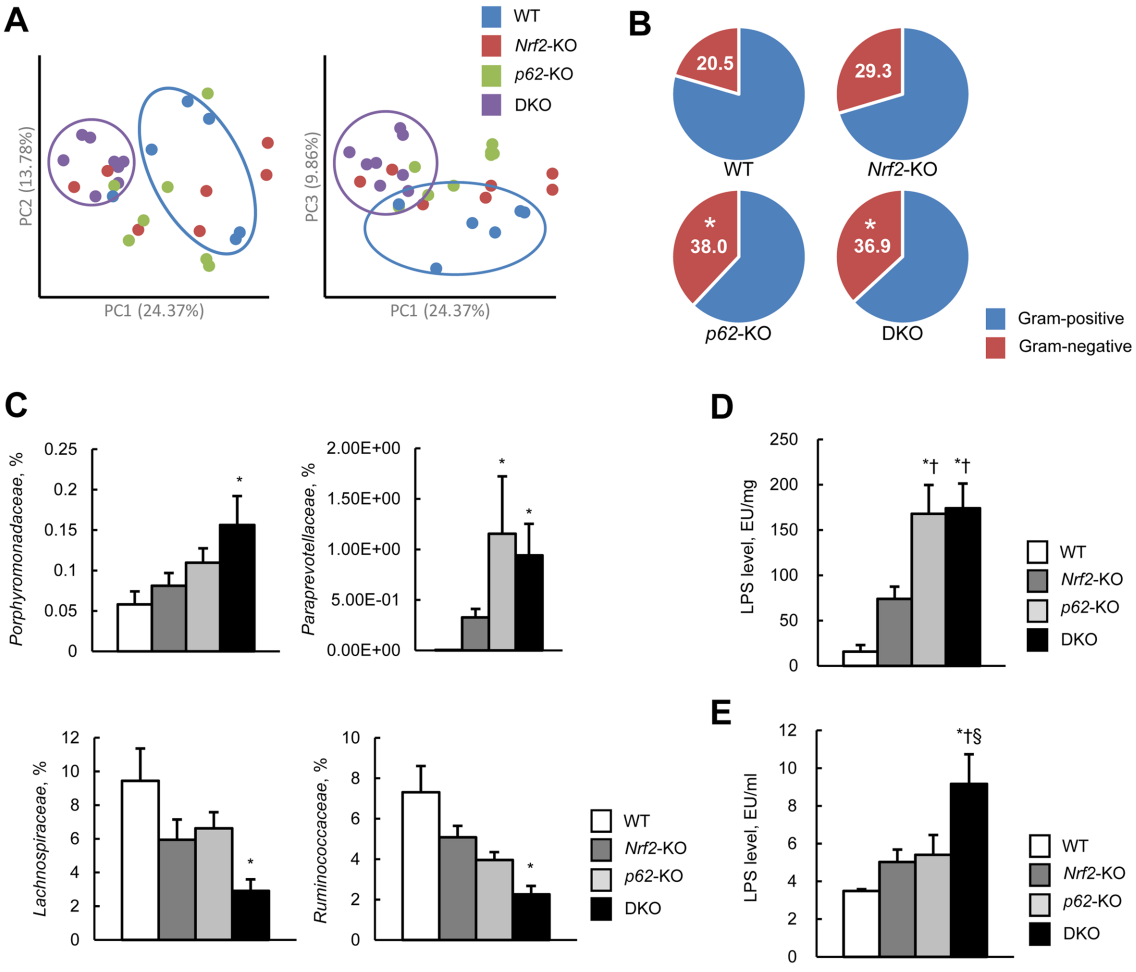

Fig. 3. *p62*:*Nrf2* gene double-knockout (DKO) mice showed a modified microbiota composition and increased fecal lipopolysaccharide (LPS) levels. (A) Principal coordinates analysis of the fecal microbiota from wild-type (WT), *Nrf2*-knockout (KO), *p62*-KO, and DKO mice at 30 weeks of age. (B) The relative abundance of gram-negative bacteria was calculated as the percentage of bacteria relative to the total bacteria for fecal bacteria (n=8 per group). (C) The relative abundance of families of bacteria in feces was examined. The relative abundance was calculated as the percentage of the bacterial subgroup relative to the total bacteria. (D) Fecal LPS levels in mice (n=8 per group). (E) Serum LPS levels in mice (n=8 per group). Results are presented as the mean ± SE. **P*<0.05, significantly different from the WT group; †*P*<0.05, significantly different from the *Nrf2*-KO group; §*P*<0.05, significantly different from the *p62*-KO group.

rier function. Compared with WT cells, TER was consistently decreased in *Nrf2*-deficient cells (Fig. 4E). The results of immunoblotting showed that the expression of Zo-1 and Claudin 1 protein decreased in *Nrf2*-deficient cells compared with WT cells (Fig. 4F). *Zo-1* mRNA expression levels decreased in *Nrf2*-deficient cells. C*laudin 1* mRNA expression levels were not significantly different (Supplementary Fig. 3B).

Because LPS causes intestinal barrier dysfunction, an *in vitro* model in which Caco-2 epithelial cells were grown in monolayers was treated with LPS. Compared with vehicle-treated cells, TER was consistently decreased in LPS-treated WT, *Nrf2*-deficient, and *p62*-deficient cells at 3 h and 6 h, indicating disruption of the barrier function in the monolayers (Fig. 4E). Of note, *Nrf2*-deficient cells potently inhibited the reduction in TER caused by treatment with LPS at all time points (Fig. 4E).

Changes in Kupffer cell phenotype in DKO mice

Macrophage polarization is a process by which macrophages express different functional programs in response to microenvironmental signals [29]. In the livers of DKO mice at 8 weeks of age, M1 phenotype Kupffer

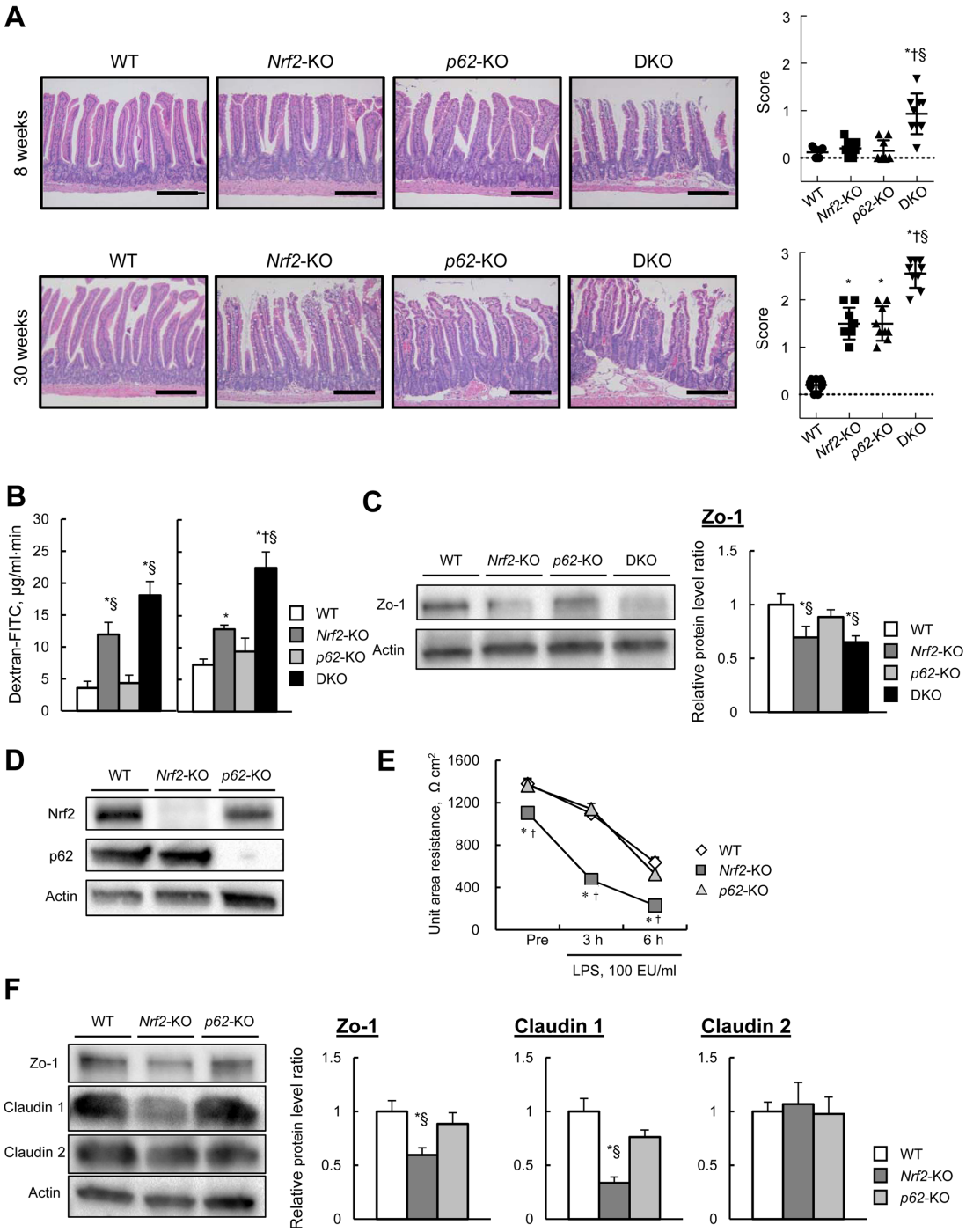

Fig. 4. Intestinal permeability increased in *p62*:*Nrf2* gene double-knockout (DKO) mice. (A) Hematoxylin and eosin (H&E)-stained sections of representative intestine specimens from wild-type (WT), *Nrf2*-knockout (KO), *p62*-KO, and DKO mice at 8 and 30 weeks of age (left panel) (scale bar, 100 μm). Histological scores for intestinal epithelia (right panel) (n=8 per group). (B) Area under the plasma concentration curve of fluorescein isothiocyanate (FITC)-dextran after administration of the marker by gavage (n=8 per group). (C) Immunoblot analysis of zona occludens-1 (Zo-1) in the intestines of WT, *Nrf2*-KO, *p62*-KO, and DKO mice at 8 weeks of age and quantification of immunoblotting of Zo-1 normalized to actin in mice (n=5 per group). (D) Immunoblot analysis of Nrf2 and p62 in Caco-2 cells of WT, *Nrf2*-KO, and *p62*-KO. (E) Barrier function was analyzed by transepithelial electrical resistance (TER). Caco-2 cells were stimulated with 100 EU/ml lipopolysaccharide (LPS) (EU, endotoxin units). TER was tested at different time points (n=5 per group). (F) Quantification of immunoblotting of Zo-1, claudin 1, and claudin 2 normalized to actin in Caco-2 cells (n=5 per group). Results are presented as the mean ± SE. **P*<0.05, significantly different from the WT group; †*P*<0.05, significantly different from the *Nrf2*-KO group; §*P*<0.05, significantly different from the *p62*-KO group.

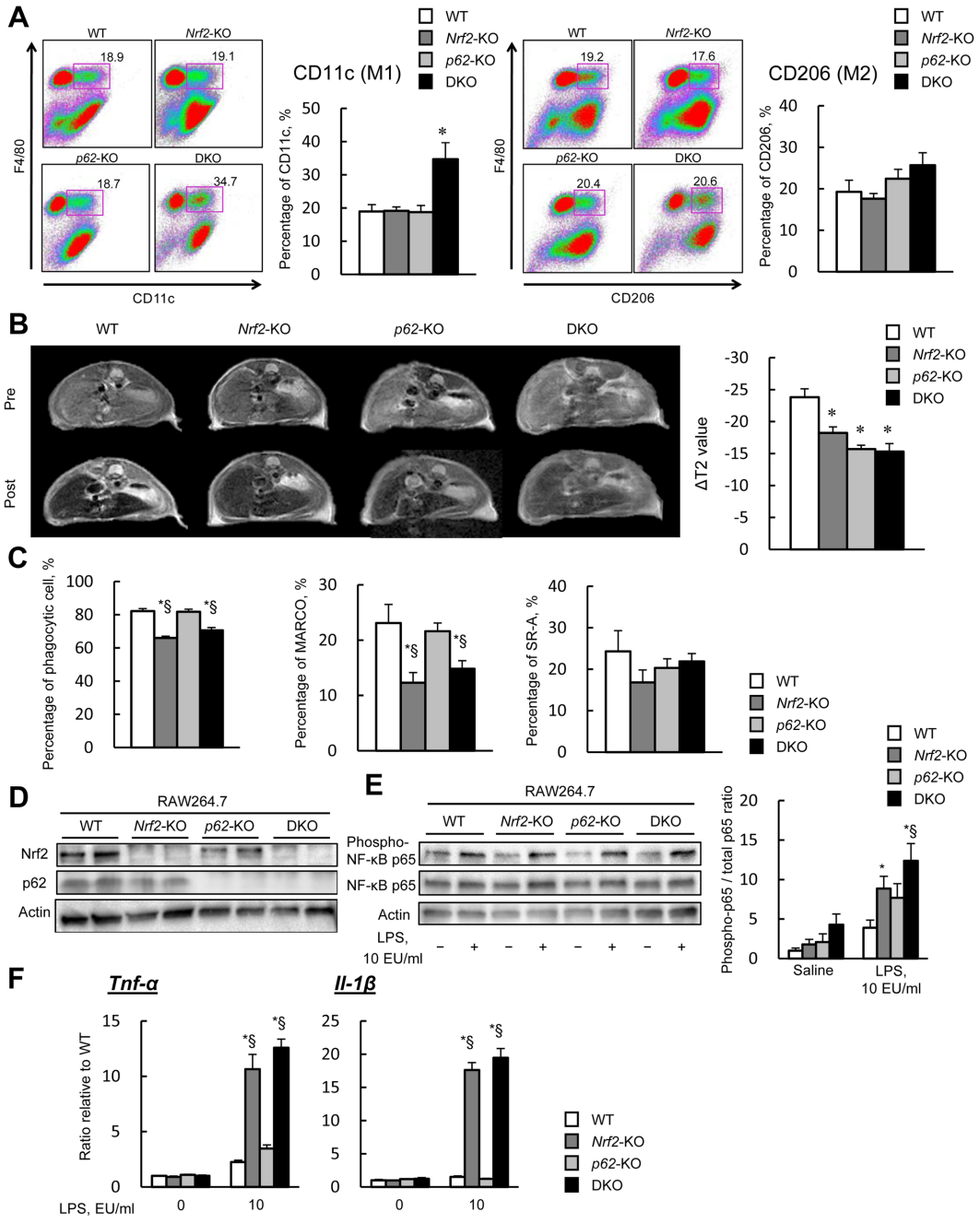

Fig. 5. Change in Kupffer cell phenotype in *p62*:*Nrf2* gene double-knockout (DKO) mice. (A) CD11c and CD206 expression in F4/80$^+$ cells (Kupffer cells) in the liver. Numbers in panels and quadrants are percentages of the indicated populations. (B) Kupffer cell phagocytic function was determined by superparamagnetic iron oxide (SPIO) magnetic resonance imaging (MRI). The SPIO signal was calculated by MRI (reflecting the T2 value), and then the phagocytic function was evaluated. (C) Phagocytic activity of F4/80$^+$ cells in the liver. Isolated liver F4/80$^+$ cells were incubated with fluorescein isothiocyanate (FITC) microspheres, and then FITC microsphere-positive cells were analyzed. MARCO and SR-A expression in F4/80$^+$ cells in the liver. (D) Immunoblot analysis of Nrf2 and p62 in RAW264.7 cells of wild-type (WT), *Nrf2*-knockout (KO), *p62*-KO, and DKO. (E) Immunoblot analysis of phosphorylated NF-kB p65 (p-NF-kB p65) and total NF-kB p65 in RAW264.7 cells of WT, *Nrf2*-KO, *p62*-KO, and DKO and quantification of immunoblotting of p-NF-kB p65 normalized to total NF-kB p65. Cells were stimulated with 10 EU/ml lipopolysaccharide (LPS) (EU, endotoxin units). Quantification of immunoblotting of p-NF-kB p65 normalized to total NF-kB p65. (F) Relative mRNA expression levels of *Tnf-α* and *IL-1β* mRNA in RAW264.7 cells (n=5 per group). mRNA expression levels were calculated as the ratio relative to that in WT cells. Results are presented as the mean ± SE. **P*<0.05, significantly different from the WT group; †*P*<0.05, significantly different from the *Nrf2*-KO group; §*P*<0.05, significantly different from the *p62*-KO group.

cells but not M2 phenotype Kupffer cells increased, as determined using flow cytometry for CD11c as a marker for M1 macrophages and CD206 as a marker for M2 macrophages (Fig. 5A).

LPS polarizes macrophages towards the M1 phenotype. M1 macrophages are implicated in the initiation and maintenance of inflammation. To directly test the inflammatory response of Kupffer cells, Kupffer cells from WT, *Nrf2*-KO, *p62*-KO, and DKO mice at 8 weeks of age were isolated and stimulated with LPS *ex vivo*. Analysis using qRT-PCR revealed that upregulation of *Tnf-α* mRNA with vehicle treatment was only present in DKO mice, indicating innate immunity activation at an early age, and that the magnitude of the upregulation was further potentiated by LPS treatment (data not shown). There was no significant difference in the number of F4/80-positive cells, which is a surface marker of Kupffer cells (Supplementary Fig. 4).

Impairment of the phagocytic function of Kupffer cells may play a critical role in the development of NASH [39, 44]. Therefore, the effects in the liver parenchymal phase were determined by SPIO-MRI, and Kupffer cell phagocytic activity was assessed in mice. The magnitude of changes in the T2 value of the liver parenchymal phase, which reflects the Kupffer cell phagocytic status of SPIO, was smaller in *Nrf2*-KO, *p62*-KO, and DKO mice than in WT mice (Fig. 5B). Simply put, the phagocytic ability decreased in these mice. When the ability of F4/80-positive cells to uptake latex beads was investigated by flow cytometry, the bead phagocytic ability was lower in *Nrf2*-KO and DKO mice than in WT and *p62*-KO mice (Fig. 5C). Correlating with these findings, the positive fraction of MARCO, a scavenger receptor, decreased in *Nrf2*-KO and DKO mice. There was no significant difference observed for the positive fraction of SR-A (Fig. 5C).

As noted, macrophages polarizing towards the M1 phenotype and innate immunity were activated in the livers of DKO mice at 8 weeks of age. The findings suggest that the Kupffer cells of DKO mice due to their genetic background accelerate the inflammatory response to excessive LPS flux through an increase in the susceptibility of innate immunity to LPS. We produced RAW264.7 lacking the *p62* or *Nrf2* gene using the CRISPR-Cas9 system. *In vitro* experiments were conducted to evaluate the inflammatory response to LPS. Expression of p62 and Nrf2 protein in each gene-deficient cell was confirmed by immunoblot analysis (Fig. 5D). Analysis showed that phosphorylation of Nuclear factor-kappa B p65 (NF-κB p65) increased in *Nrf2*-deficient cells compared with WT cells (Fig. 5E). Interestingly, *Tnf-α* and *IL-1β* mRNA expression levels following treatment with low-dose LPS were also upregulated in *Nrf2*-deficient cells compared with WT cells (Fig. 5F).

Diet restriction improved NASH in DKO mice

To confirm the association between hyperphagia-induced obesity and NASH development in DKO mice, diet restriction by pair-feeding was conducted using DKO mice. Pair-feeding restricted the intake of standard chow to 3.0 ± 0.1 g/day/mouse. DKO mice subjected to diet restriction showed a body weight gain curve similar to WT mice fed *ad libitum* (Fig. 6A). When compared with *ad libitum* DKO mice with liver steatosis, inflammation, and fibrosis, pair-feed DKO mice showed dramatic improvements in these pathological conditions in the liver (Figs. 6B and C). Improvements in NASH conditions were coupled with recovered intestinal permeability (Fig. 6D) and improved microbiota composition (e.g., a decreased proportion of gram-negative bacteria and decreased fecal LPS concentrations) (Fig. 6E) and thereby decreased serum LPS concentrations (Fig. 6F).

Discussion

The major findings of this study are that *p62* deficiency resulted in hyperphagia-induced obesity coupled with insulin resistance and adipokine imbalance as well as dysbiosis and that *Nrf2* deficiency resulted in intestinal barrier dysfunction and an accelerated inflammatory response to LPS in Kupffer cells. Both defects resulted in the onset and progression of NASH and were associated with hepatic tumorigenesis in DKO mice fed a normal diet. However, *p62* or *Nrf2* single gene-knockout mice did not progress to NASH.

Of note, in DKO mice, a high-fat diet is not needed for the development of NASH. In this regard, inflammatory events may lead to fat accumulation (steatosis) in the livers [26]. As proposed by the multiple parallel hits theory, which is currently accepted as the pathogenesis of nonalcoholic fatty liver disease (NAFLD) [38], inflammatory mediators from the intestines (e.g., LPS) and adipose tissue (e.g., adipokines) could play a central role in the cascade of hepatic inflammation and fibrosis development. It is possible that, in DKO mice, activation

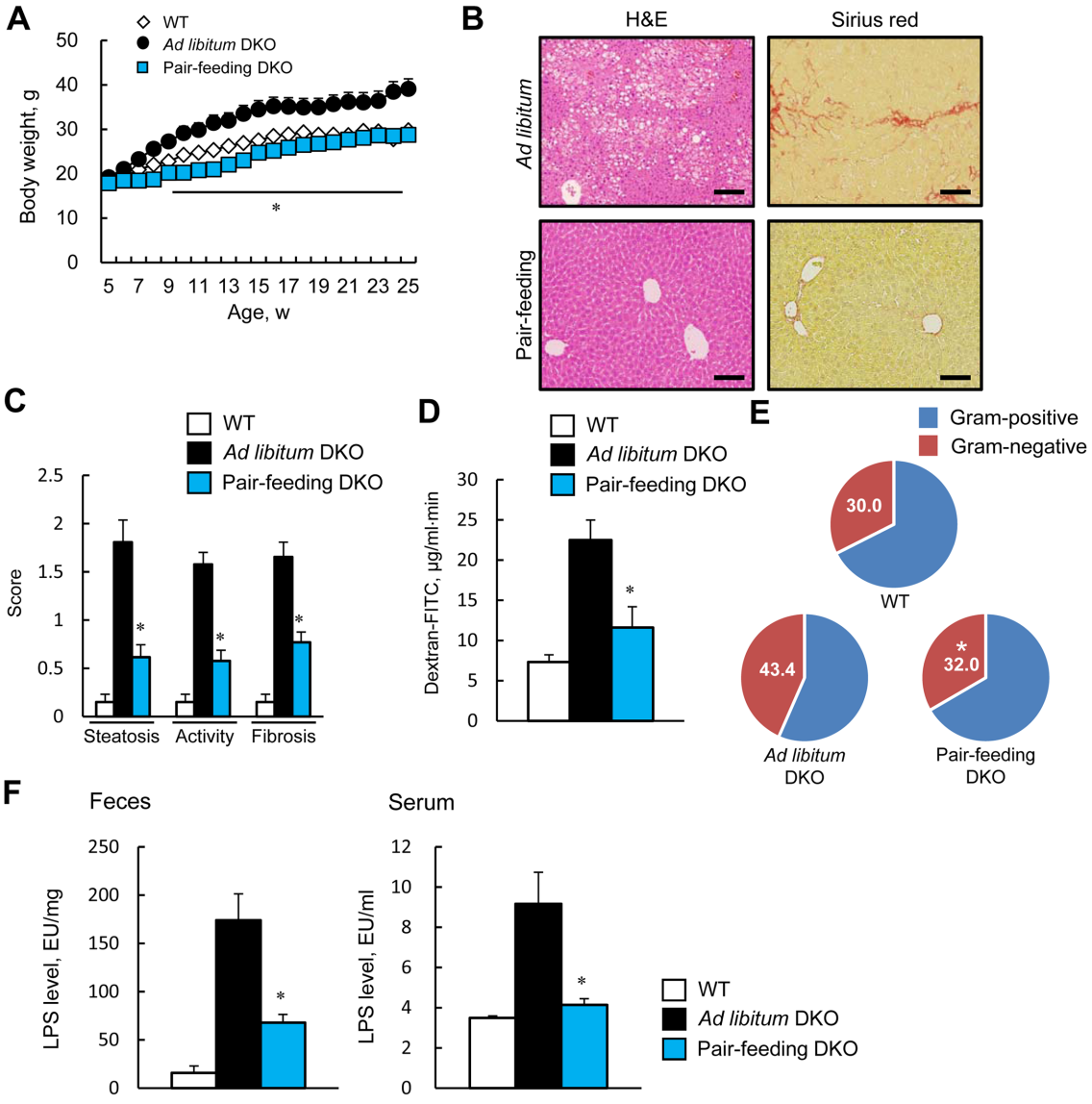

Fig. 6. Diet restriction improved nonalcoholic steatohepatitis (NASH) in *p62*:*Nrf2* gene double-knockout (DKO) mice. (A) Body weight changes in wild-type (WT), *ad libitum* DKO, and pair-feeding mice (n=10–15 per group). (B) Hematoxylin and eosin (H&E)- and sirius red-stained sections of representative liver specimens from the *ad libitum* DKO and pair-feeding groups at 30 weeks of age (scale bar, 100 μm). (C) The steatosis, activity, and fibrosis (SAF) scores for each group are shown (8 per group). (D) Area under the plasma concentration curve of fluorescein isothiocyanate (FITC)-dextran in plasma after administration of the marker by gavage (n=8 per group). (E) The relative abundance of gram-negative bacteria was calculated as the percentage of bacteria relative to the total bacteria for fecal bacteria (n=8 per group). (F) Fecal and serum lipopolysaccharide (LPS) levels in WT, *ad libitum* DKO, and pair-feeding mice (n=8 per group). Results are presented as the mean ± SE. **P*<0.05, significantly different from the *ad libitum* DKO group.

of innate immunity by an excessive LPS flux, occurring both within and outside the liver, is a central pathway that regulates the development of hepatic damage in the form of NASH.

Cumulative data suggests that dysbiosis of the intestinal microbiota is associated with the onset and progression of NASH [9]. Several studies have reported that serum LPS levels are elevated in NAFLD patients compared with controls [14, 25]. The fecal microbiota in NAFLD or NASH patients has been assessed using culture-independent techniques such as sequencing of a conserved region in the bacterial 16S rRNA gene. Microbiota samples from patients with NAFLD or NASH have a higher proportion of members of the *Porphyro-*

monadaceae family and a lower proportion of members of the *Lachnospiraceae* and *Ruminococcaceae* families than those from healthy people [42, 47]. Flora analysis of DKO mice in the current study showed an increased proportion of *Porphyromonadaceae* and decreased proportions of *Lachnospiraceae* and *Ruminococcaceae* (Fig. 3). Because we compared proportions of microflora, it is impossible to accurately compare the number of bacteria. The fecal LPS concentration was elevated in both *p62*-KO and DKO mice. However, serum LPS concentrations were elevated only in DKO mice. Interestingly, diet restriction by pair-feeding decreased fecal and serum LPS concentrations in DKO mice, which in turns resulted in an improvement in the hepatic conditions of NASH (Fig. 6). Moreover, administration of the probiotic VSL#3 from 10 to 25 weeks of age increased the bacterial species *Bifidobacterium infantis* and *Streptococcus thermophilus* in feces and reduced serum LPS concentrations (Supplemental Figs. 5A and 5B). In addition, steatosis, inflammation, and fibrosis were improved in the liver (Supplemental Fig. 5C). From these results, it is suggested that *p62* deficiency in DKO mice modifies the intestinal flora (e.g., increasing the proportion of gram-negative bacteria) through hyperphagia and thereby increases fecal LPS concentrations. In addition, the activation of TLR4 by LPS from intestinal Gram-negative bacteria has recently been shown to promote the development of hepatocellular carcinoma [6]. Therefore, it is likely that in DKO mice LPS is closely involved in the liver tumorigenesis, since the expression levels of genes downstream of TLR4 were increased in the liver (Table 1).

Previous studies suggest a pathological link between intestinal permeability status and NASH. It is reported that the intestinal microbiome is perturbed in both people with obesity and NAFLD patients, which in turn may lead to increased fecal LPS levels and result in leaky gut [41]. Luca *et al*. reported that intestinal permeability is increased in patients with NAFLD and that the staining intensity of Zo-1 in the intestinal epithelia significantly decreases in patients with NAFLD [30]. The results of the current study (Fig. 4) indicate that both *Nrf2* deficiency in mice and *Nrf2* deletion in Caco-2 cells contribute to increased intestinal permeability through a decrease in Zo-1 expression levels, suggesting that Nrf2 is closely involved in the maintenance of intestinal barrier function. In addition, Nrf2 is known to inhibit the expression levels of i-nitric oxide synthase [27]. Therefore, in the damaged intestines of DKO mice (Fig. 4), an LPS-induced increase in inducible NO synthase activity may also be an important factor responsible for the increased permeability as reported previously [11].

Obesity is an inflammatory condition characterized by increased activity of the innate immune system. Increased sensitivity of the liver to LPS in people with obesity is closely associated with the pathogenesis of NASH [43]. Understanding the role of Kupffer cells in the context of inflammation in the pathogenetic process of LPS-induced liver injury has recently increased. Imajo *et al*. demonstrated that obesity-associated increases in leptin levels result in an increased sensitivity of Kupffer cells to low doses of LPS through increased expression of CD14, a receptor for LPS and LPS-binding protein complexes [16]. In the current study, increased leptin levels in DKO mice at 8 and 30 weeks of age were associated with increased expression levels of pro-inflammatory cytokines in the liver at 8 and 30 weeks of age and those in visceral fat at 30 weeks of age (Table 1).

Activation of innate immunity may play a role in the pathophysiology of inflammation-induced liver damage. Kupffer cells play an important role in innate immunity. Macrophages (Kupffer cells) undergo specific differentiation depending on the local tissue environment, responding to environmental cues within tissues such as damaged cells or microbial products to differentiate into distinct functional phenotypes. In the current study, phenotypic changes in Kupffer cells were observed in DKO mice (Fig. 5), with the proportion of M1 phenotype Kupffer cells increasing. The M1 macrophage phenotype, which is characterized by the production of high levels of pro-inflammatory cytokines and high production of reactive nitrogen and oxygen intermediates, is implicated in initiation and maintenance of inflammation. Therefore, the phenotypic changes are thought to worsen the hepatic conditions of NASH [1].

The responsiveness of cultured macrophages to low doses of LPS increased with *Nrf2* deletion in the current study (Fig. 5). Activation of Nrf2 prevents LPS-induced upregulation of pro-inflammatory cytokines [22]. Therefore, an increased inflammatory response to low doses of LPS in *Nrf2* deficiency and hyperleptinemia in *p62* deficiency are closely associated with maintenance of inflammation in the livers of DKO mice.

In this study, the phagocytic ability of Kupffer cells decreased in DKO mice. Flow cytometry revealed that

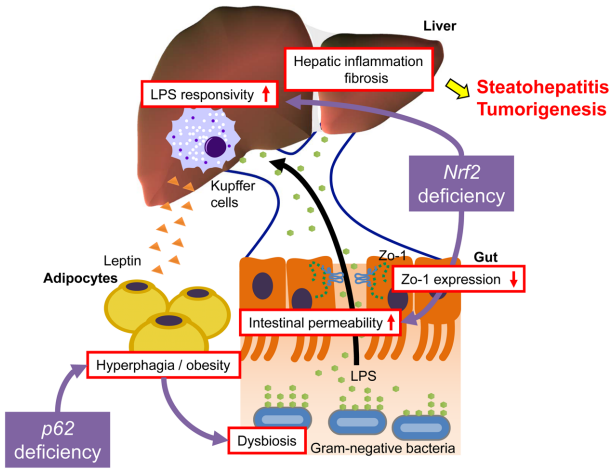

Fig. 7. Summary of nonalcoholic steatohepatitis in *p62:Nrf2* double-knockout (DKO) mice.

Nrf2 deficiency reduced the expression level of MARCO as a scavenger receptor and decreased the phagocytic ability of Kupffer cells (Fig. 5). In humans and rats, impaired phagocytic functions of Kupffer cells are causatively associated with the development of NASH [39]. MARCO restricts TLR4 responses to LPS, and expression levels of MARCO increase when LPS is administered [31]. Therefore, decreased expression of MARCO in DKO mice may increase the TLR4 response to low doses of LPS.

Several studies have reported the involvement of p62 and NRF2 in human NASH. p62 is a component of Mallory-Denk bodies, which are protein aggregates that accumulate in damaged liver cells in NASH, cirrhosis, and HCC [36]. Impaired autophagic flux is associated with increased endoplasmic reticulum stress during the development of NASH, and consequently, levels of hepatic p62 protein are significantly increased in patients with NASH compared with those in control subjects [10]. In contrast, Duran *et al.* showed that p62 expression was significantly lower in tumoral hepatic stellate cells, causing impaired repression of fibrosis and inflammation [8]. Activation of NRF2 is also observed in human NASH [13, 21], indicating that NRF2 plays an important role in adaptation to oxidative stress in NASH and tumors. These reports indicate that p62 and NRF2 may have important roles in human NASH progression.

In conclusion, feeding of a standard diet to DKO mice resulted in the development of NASH and was associated with tumorigenesis. *In vivo* and *in vitro* studies revealed that *p62* deficiency resulted in hyperphagia-induced obesity coupled with insulin resistance and adipokine imbalance as well as dysbiosis (e.g., an increased proportion of gram-negative bacteria) and that *Nrf2* deficiency resulted in intestinal barrier dysfunction and an accelerated inflammatory response to LPS in Kupffer cells. In mice, activation of innate immunity by excessive LPS flux, occurring both within and outside the liver (e.g., intestines and visceral adipose tissue), is central to the development of hepatic damage in the form of NASH (Fig. 7). Because of the phenotypic similarities to the clinical features of human NASH, e.g., obesity (visceral fat accumulation) coupled with metabolic syndrome, insulin resistance, and adipokine imbalance, DKO mice represent a unique animal model for investigating the pathogenesis of human NASH and exploring novel targets for the prevention and/or treatment of NASH. A therapeutic approach targeting the intestinal flora and intestinal barrier function with probiotics may be useful for the potential management of NASH.

Author Contributions

K.A., E.W., K.O., and J.S. developed the study concept and experimental design. K.A. performed all animal study procedures and most in vitro experiments. K.T. scored mouse livers for the features of NASH. T.Y., T.I., and K.K. helped with the design and interpreting the results. K.A., E.W., K.O., and J.S. interpreted the data and wrote the manuscript.

Conflict of Interest

The authors declare that they have no potential conflicts of interest.

Acknowledgments

This work was supported in part by Grants-in-Aid for Scientific Research from the Ministry of Education, Culture, Sports, Science and Technology, Japan (No. 25282212, 26282191, 26293284, 26293297, 15H04917, 15K15037, 15K15488, 16J00793, 16K15188, 17H02174, 17K19887, and 17K19888), and a Grant-in-Aid from the Nakayama Cancer Research Institute (Tokyo, Japan). We would like to thank all our co-workers who supported this work at our institution. We would also like to thank Naohiro Gotoh (Department of Food Science and Technology, Tokyo University of Marine Science

and Technology, Tokyo, Japan), Toru Kawamoto (Faculty of Medicine, Tokyo Women's Medical University, Tokyo, Japan), Tetsuya Ueda (Drug Development Service Division, Pharmacodynamics Group, Medi-chem Business Segment, LSI Medience Corporation, Tokyo, Japan), Tomoyuki Haishi (MRTechnology, Inc., Ibaraki, Japan), and Masayuki Yamamoto (Department of Medical Biochemistry, Tohoku University Graduate School of Medicine, Miyagi, Japan).

References

1. Baffy, G. 2009. Kupffer cells in non-alcoholic fatty liver disease: the emerging view. *J. Hepatol.* 51: 212–223. [Medline] [CrossRef]
2. Bedossa, P. 2017. Pathology of non-alcoholic fatty liver disease. *Liver Int.* 37:(Suppl 1): 85–89. [Medline] [CrossRef]
3. Bugianesi, E., Leone, N., Vanni, E., Marchesini, G., Brunello, F., Carucci, P., Musso, A., De Paolis, P., Capussotti, L., Salizzoni, M., and Rizzetto, M. 2002. Expanding the natural history of nonalcoholic steatohepatitis: from cryptogenic cirrhosis to hepatocellular carcinoma. *Gastroenterology* 123: 134–140. [Medline] [CrossRef]
4. Chitturi, S. and Farrell, G.C. 2001. Etiopathogenesis of nonalcoholic steatohepatitis. *Semin. Liver Dis.* 21: 27–41. [Medline] [CrossRef]
5. Cong, L., Ran, F.A., Cox, D., Lin, S., Barretto, R., Habib, N., Hsu, P.D., Wu, X., Jiang, W., Marraffini, L.A., and Zhang, F. 2013. Multiplex genome engineering using CRISPR/Cas systems. *Science* 339: 819–823. [Medline] [CrossRef]
6. Dapito, D.H., Mencin, A., Gwak, G.Y., Pradere, J.P., Jang, M.K., Mederacke, I., Caviglia, J.M., Khiabanian, H., Adeyemi, A., Bataller, R., Lefkowitch, J.H., Bower, M., Friedman, R., Sartor, R.B., Rabadan, R., and Schwabe, R.F. 2012. Promotion of hepatocellular carcinoma by the intestinal microbiota and TLR4. *Cancer Cell* 21: 504–516. [Medline] [CrossRef]
7. Day, C.P. and James, O.F. 1998. Steatohepatitis: a tale of two "hits"? *Gastroenterology* 114: 842–845. [Medline] [CrossRef]
8. Duran, A., Hernandez, E.D., Reina-Campos, M., Castilla, E.A., Subramaniam, S., Raghunandan, S., Roberts, L.R., Kisseleva, T., Karin, M., Diaz-Meco, M.T., and Moscat, J. 2016. p62/SQSTM1 by Binding to Vitamin D Receptor Inhibits Hepatic Stellate Cell Activity, Fibrosis, and Liver Cancer. *Cancer Cell* 30: 595–609. [Medline] [CrossRef]
9. Gkolfakis, P., Dimitriadis, G., and Triantafyllou, K. 2015. Gut microbiota and non-alcoholic fatty liver disease. *Hepatobiliary Pancreat. Dis. Int.* 14: 572–581. [Medline]
10. González-Rodríguez, A., Mayoral, R., Agra, N., Valdecantos, M.P., Pardo, V., Miquilena-Colina, M.E., Vargas-Castrillón, J., Lo Iacono, O., Corazzari, M., Fimia, G.M., Piacentini, M., Muntané, J., Boscá, L., García-Monzón, C., Martín-Sanz, P., and Valverde, A.M. 2014. Impaired autophagic flux is associated with increased endoplasmic reticulum stress during the development of NAFLD. *Cell Death Dis.* 5: e1179. [Medline] [CrossRef]
11. Han, X., Fink, M.P., Yang, R., and Delude, R.L. 2004. Increased iNOS activity is essential for intestinal epithelial tight junction dysfunction in endotoxemic mice. *Shock* 21: 261–270. [Medline] [CrossRef]
12. Harada, H., Warabi, E., Matsuki, T., Yanagawa, T., Okada, K., Uwayama, J., Ikeda, A., Nakaso, K., Kirii, K., Noguchi, N., Bukawa, H., Siow, R.C., Mann, G.E., Shoda, J., Ishii, T., and Sakurai, T. 2013. Deficiency of p62/Sequestosome 1 causes hyperphagia due to leptin resistance in the brain. *J. Neurosci.* 33: 14767–14777. [Medline] [CrossRef]
13. Hardwick, R.N., Fisher, C.D., Canet, M.J., Lake, A.D., and Cherrington, N.J. 2010. Diversity in antioxidant response enzymes in progressive stages of human nonalcoholic fatty liver disease. *Drug Metab. Dispos.* 38: 2293–2301. [Medline] [CrossRef]
14. Harte, A.L., da Silva, N.F., Creely, S.J., McGee, K.C., Billyard, T., Youssef-Elabd, E.M., Tripathi, G., Ashour, E., Abdalla, M.S., Sharada, H.M., Amin, A.I., Burt, A.D., Kumar, S., Day, C.P., and McTernan, P.G. 2010. Elevated endotoxin levels in non-alcoholic fatty liver disease. *J. Inflamm. (Lond.)* 7: 15. [Medline] [CrossRef]
15. Horie, Y., Suzuki, A., Kataoka, E., Sasaki, T., Hamada, K., Sasaki, J., Mizuno, K., Hasegawa, G., Kishimoto, H., Iizuka, M., Naito, M., Enomoto, K., Watanabe, S., Mak, T.W., and Nakano, T. 2004. Hepatocyte-specific Pten deficiency results in steatohepatitis and hepatocellular carcinomas. *J. Clin. Invest.* 113: 1774–1783. [Medline] [CrossRef]
16. Imajo, K., Fujita, K., Yoneda, M., Nozaki, Y., Ogawa, Y., Shinohara, Y., Kato, S., Mawatari, H., Shibata, W., Kitani, H., Ikejima, K., Kirikoshi, H., Nakajima, N., Saito, S., Maeyama, S., Watanabe, S., Wada, K., and Nakajima, A. 2012. Hyperresponsivity to low-dose endotoxin during progression to nonalcoholic steatohepatitis is regulated by leptin-mediated signaling. *Cell Metab.* 16: 44–54. [Medline] [CrossRef]
17. Ishii, T., Yanagawa, T., Kawane, T., Yuki, K., Seita, J., Yoshida, H., and Bannai, S. 1996. Murine peritoneal macrophages induce a novel 60-kDa protein with structural similarity to a tyrosine kinase p56lck-associated protein in response to oxidative stress. *Biochem. Biophys. Res. Commun.* 226: 456–460. [Medline] [CrossRef]
18. Itoh, K., Chiba, T., Takahashi, S., Ishii, T., Igarashi, K., Katoh, Y., Oyake, T., Hayashi, N., Satoh, K., Hatayama, I., Yamamoto, M., and Nabeshima, Y. 1997. An Nrf2/small Maf heterodimer mediates the induction of phase II detoxifying enzyme genes through antioxidant response elements. *Biochem. Biophys. Res. Commun.* 236: 313–322. [Medline] [CrossRef]
19. Itoh, K., Igarashi, K., Hayashi, N., Nishizawa, M., and Yamamoto, M. 1995. Cloning and characterization of a novel erythroid cell-derived CNC family transcription factor heterodimerizing with the small Maf family proteins. *Mol. Cell. Biol.* 15: 4184–4193. [Medline] [CrossRef]
20. Itoh, K., Mimura, J., and Yamamoto, M. 2010. Discovery of the negative regulator of Nrf2, Keap1: a historical overview. *Antioxid. Redox Signal.* 13: 1665–1678. [Medline] [CrossRef]

21. Kakehashi, A., Stefanov, V.E., Ishii, N., Okuno, T., Fujii, H., Kawai, K., Kawada, N., and Wanibuchi, H. 2017. Proteome characteristics of non-alcoholic steatohepatitis liver tissue and associated hepatocellular carcinomas. *Int. J. Mol. Sci.* 18: 18. [Medline] [CrossRef]
22. Kobayashi, E.H., Suzuki, T., Funayama, R., Nagashima, T., Hayashi, M., Sekine, H., Tanaka, N., Moriguchi, T., Motohashi, H., Nakayama, K., and Yamamoto, M. 2016. Nrf2 suppresses macrophage inflammatory response by blocking proinflammatory cytokine transcription. *Nat. Commun.* 7: 11624. [Medline] [CrossRef]
23. Kobayashi, M. and Yamamoto, M. 2006. Nrf2-Keap1 regulation of cellular defense mechanisms against electrophiles and reactive oxygen species. *Adv. Enzyme Regul.* 46: 113–140. [Medline] [CrossRef]
24. Komatsu, M., Waguri, S., Koike, M., Sou, Y.S., Ueno, T., Hara, T., Mizushima, N., Iwata, J., Ezaki, J., Murata, S., Hamazaki, J., Nishito, Y., Iemura, S., Natsume, T., Yanagawa, T., Uwayama, J., Warabi, E., Yoshida, H., Ishii, T., Kobayashi, A., Yamamoto, M., Yue, Z., Uchiyama, Y., Kominami, E., and Tanaka, K. 2007. Homeostatic levels of p62 control cytoplasmic inclusion body formation in autophagy-deficient mice. *Cell* 131: 1149–1163. [Medline] [CrossRef]
25. Kudo, H., Takahara, T., Yata, Y., Kawai, K., Zhang, W., and Sugiyama, T. 2009. Lipopolysaccharide triggered TNF-alpha-induced hepatocyte apoptosis in a murine non-alcoholic steatohepatitis model. *J. Hepatol.* 51: 168–175. [Medline] [CrossRef]
26. Li, Z., Yang, S., Lin, H., Huang, J., Watkins, P.A., Moser, A.B., Desimone, C., Song, X.Y., and Diehl, A.M. 2003. Probiotics and antibodies to TNF inhibit inflammatory activity and improve nonalcoholic fatty liver disease. *Hepatology* 37: 343–350. [Medline] [CrossRef]
27. Lin, W., Wu, R.T., Wu, T., Khor, T.O., Wang, H., and Kong, A.N. 2008. Sulforaphane suppressed LPS-induced inflammation in mouse peritoneal macrophages through Nrf2 dependent pathway. *Biochem. Pharmacol.* 76: 967–973. [Medline] [CrossRef]
28. Ling, X., Linglong, P., Weixia, D., and Hong, W. 2016. Protective effects of bifidobacterium on intestinal barrier function in LPS-induced enterocyte barrier injury of Caco-2 monolayers and in a rat NEC model. *PLoS One* 11: e0161635. [Medline] [CrossRef]
29. Mantovani, A., Sozzani, S., Locati, M., Allavena, P., and Sica, A. 2002. Macrophage polarization: tumor-associated macrophages as a paradigm for polarized M2 mononuclear phagocytes. *Trends Immunol.* 23: 549–555. [Medline] [CrossRef]
30. Miele, L., Valenza, V., La Torre, G., Montalto, M., Cammarota, G., Ricci, R., Mascianà, R., Forgione, A., Gabrieli, M.L., Perotti, G., Vecchio, F.M., Rapaccini, G., Gasbarrini, G., Day, C.P., and Grieco, A. 2009. Increased intestinal permeability and tight junction alterations in nonalcoholic fatty liver disease. *Hepatology* 49: 1877–1887. [Medline] [CrossRef]
31. Mukhopadhyay, S., Varin, A., Chen, Y., Liu, B., Tryggvason, K., and Gordon, S. 2011. SR-A/MARCO-mediated ligand delivery enhances intracellular TLR and NLR function, but ligand scavenging from cell surface limits TLR4 response to pathogens. *Blood* 117: 1319–1328. [Medline] [CrossRef]
32. Okada, K., Warabi, E., Sugimoto, H., Horie, M., Gotoh, N., Tokushige, K., Hashimoto, E., Utsunomiya, H., Takahashi, H., Ishii, T., Yamamoto, M., and Shoda, J. 2013. Deletion of Nrf2 leads to rapid progression of steatohepatitis in mice fed atherogenic plus high-fat diet. *J. Gastroenterol.* 48: 620–632. [Medline] [CrossRef]
33. Rodriguez, A., Durán, A., Selloum, M., Champy, M.F., Diez-Guerra, F.J., Flores, J.M., Serrano, M., Auwerx, J., Diaz-Meco, M.T., and Moscat, J. 2006. Mature-onset obesity and insulin resistance in mice deficient in the signaling adapter p62. *Cell Metab.* 3: 211–222. [Medline] [CrossRef]
34. Scarpellini, E., Lupo, M., Iegri, C., Gasbarrini, A., De Santis, A., and Tack, J. 2014. Intestinal permeability in non-alcoholic fatty liver disease: the gut-liver axis. *Rev. Recent Clin. Trials* 9: 141–147. [Medline]
35. Shin, J. 1998. P62 and the sequestosome, a novel mechanism for protein metabolism. *Arch. Pharm. Res.* 21: 629–633. [Medline] [CrossRef]
36. Stumptner, C., Fuchsbichler, A., Zatloukal, K., and Denk, H. 2007. In vitro production of Mallory bodies and intracellular hyaline bodies: the central role of sequestosome 1/p62. *Hepatology* 46: 851–860. [Medline] [CrossRef]
37. Thimmulappa, R.K., Lee, H., Rangasamy, T., Reddy, S.P., Yamamoto, M., Kensler, T.W., and Biswal, S. 2006. Nrf2 is a critical regulator of the innate immune response and survival during experimental sepsis. *J. Clin. Invest.* 116: 984–995. [Medline] [CrossRef]
38. Tilg, H. and Moschen, A.R. 2010. Evolution of inflammation in nonalcoholic fatty liver disease: the multiple parallel hits hypothesis. *Hepatology* 52: 1836–1846. [Medline] [CrossRef]
39. Tonan, T., Fujimoto, K., Qayyum, A., Morita, Y., Nakashima, O., Ono, N., Kawahara, A., Kage, M., Hayabuchi, N., and Ueno, T. 2012. CD14 expression and Kupffer cell dysfunction in non-alcoholic steatohepatitis: superparamagnetic iron oxide-magnetic resonance image and pathologic correlation. *J. Gastroenterol. Hepatol.* 27: 789–796. [Medline] [CrossRef]
40. Vuppalanchi, R. and Chalasani, N. 2009. Nonalcoholic fatty liver disease and nonalcoholic steatohepatitis: Selected practical issues in their evaluation and management. *Hepatology* 49: 306–317. [Medline] [CrossRef]
41. Wigg, A.J., Roberts-Thomson, I.C., Dymock, R.B., McCarthy, P.J., Grose, R.H., and Cummins, A.G. 2001. The role of small intestinal bacterial overgrowth, intestinal permeability, endotoxaemia, and tumour necrosis factor alpha in the pathogenesis of non-alcoholic steatohepatitis. *Gut* 48: 206–211. [Medline] [CrossRef]
42. Wong, V.W., Tse, C.H., Lam, T.T., Wong, G.L., Chim, A.M., Chu, W.C., Yeung, D.K., Law, P.T., Kwan, H.S., Yu, J., Sung, J.J., and Chan, H.L. 2013. Molecular characterization of the fecal microbiota in patients with nonalcoholic steatohepatitis--a longitudinal study. *PLoS One* 8: e62885. [Medline] [CrossRef]
43. Yang, S.Q., Lin, H.Z., Lane, M.D., Clemens, M., and Diehl, A.M. 1997. Obesity increases sensitivity to endotoxin liver

injury: implications for the pathogenesis of steatohepatitis. *Proc. Natl. Acad. Sci. USA* 94: 2557–2562. [Medline] [CrossRef]

44. Yoshikawa, S., Iijima, H., Saito, M., Tanaka, H., Imanishi, H., Yoshimoto, N., Yoshimoto, T., Futatsugi-Yumikura, S., Nakanishi, K., Tsujimura, T., Nishigami, T., Kudo, A., Arii, S., and Nishiguchi, S. 2010. Crucial role of impaired Kupffer cell phagocytosis on the decreased Sonazoid-enhanced echogenicity in a liver of a nonalchoholic steatohepatitis rat model. *Hepatol. Res.* 40: 823–831. [Medline] [CrossRef]
45. Zhang, B.H., Weltman, M., and Farrell, G.C. 1999. Does steatohepatitis impair liver regeneration? A study in a dietary model of non-alcoholic steatohepatitis in rats. *J. Gastroenterol. Hepatol.* 14: 133–137. [Medline] [CrossRef]
46. Zhao, L.F., Jia, J.M., and Han, D.W. 2004. [The role of enterogenous endotoxemia in the pathogenesis of non-alcoholic steatohepatitis]. *Zhonghua Gan Zang Bing Za Zhi* 12: 632. (in Chinese) [Medline]
47. Zhu, L., Baker, S.S., Gill, C., Liu, W., Alkhouri, R., Baker, R.D., and Gill, S.R. 2013. Characterization of gut microbiomes in nonalcoholic steatohepatitis (NASH) patients: a connection between endogenous alcohol and NASH. *Hepatology* 57: 601–609. [Medline] [CrossRef]